2019

Implementation and Comparison of Active and Reactive Power Flow Control Methods in a Single Phase Grid-Connected Microgrid

Kanavaros, Dimitrios; Oriti, Giovanna; Julian, Alexander L.

IEEE

Kanavaros, Dimitrios, Giovanna Oriti, and Alexander L. Julian. "Implementation and comparison of active and reactive power flow control methods in a single phase grid-connected microgrid." 2019 IEEE Energy Conversion Congress and Exposition (ECCE). IEEE, 2019.

http://hdl.handle.net/10945/65811

Implementation and Comparison of Active and Reactive Power Flow Control Methods in a Single Phase Grid-Connected Microgrid

Dimitrios Kanavaros
Electrical and Computer Engineering Dept.
Naval Postgraduate School
Monterey, CA, USA
kanabaros_dimitris@yahoo.gr

Giovanna Oriti
Electrical and Computer Engineering Dept.
Naval Postgraduate School
Monterey, CA, USA
goriti@nps.edu

Alexander L. Julian
Consultant
Seaside, CA, USA
alexander.julian@ieee.org

***Abstract*— Grid-connected inverters are essential microgrid components that interface a common DC bus, fed by several distributed resources, to the AC loads. This paper presents different methods to control active and reactive power flow from the AC source in a single phase microgrid when it operates in grid-connected mode. A novel Direct-Quadrature (DQ) frame control strategy is presented and its performance evaluated using different methods to produce the orthogonal axis components. The different strategies are presented and compared with respect to their static performance. Physics-based models and simulated plots are presented and validated by experimental waveforms measured on a laboratory prototype.**

Keywords—energy management system; active power control; reactive power control; microgrid; power factor.

I. INTRODUCTION

The necessity of electric power 24 hours per day all over the world has led to the pervasive use of Distributed Energy Resources (DERs) including generators, solar panels, and energy storage systems, such as batteries. DERs are often controlled to form a microgrid to ensure that electricity is available to an installation when the main grid is off. Microgrid is a synthesized word from micro (the origin of the word micro is the Greek word *mikros*, which means small) and grid, indicating that a microgrid is a miniature of the main grid with the main purpose to operate autonomously to increase the reliability of a local power system.

The control of the DERs and loads in a microgrid can be established by an energy management system (EMS), a power electronics-based system which not only manages the microgrid's DERs and loads, but can also detect when the main grid is off and controls whether the microgrid operates in grid-connected mode or in islanding mode (disconnected from the main AC grid) [1]-[3]. An overview of the EMS-controlled single phase microgrid considered in this paper is shown in Fig. 1, where the AC bus controller is either a voltage-mode regulator during the islanding mode of operation or a current-mode regulator during the grid-connected mode of operation. In this microgrid representation critical loads are those loads that are crucial for the operation of the installation and must be powered at all times.

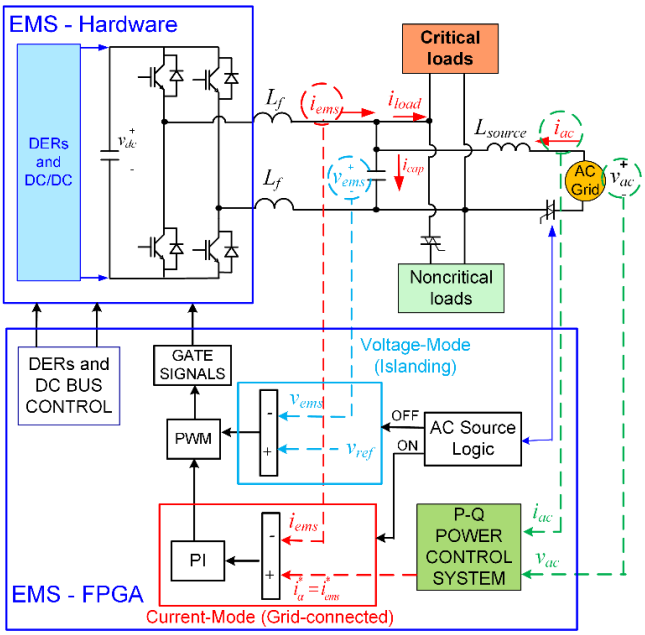

Fig. 1. EMS with focus on the AC bus control system.

The EMS provides ancillary services such as reactive power control [3], which can be implemented in many ways, with and without the use of Direct-Quadrature (DQ) frame [4]-[8]. Although many DQ control strategies have been reported in previous literature for single phase inverters, for both grid-connected [4][5] and islanding mode of operation [6][7], no previous work compares them, except in a qualitative way [6], therefore making it challenging for engineers to appreciate the differences between orthogonal generation methods (OGMs). The novel contribution of this paper includes a detailed analysis of the impact that four OGMs have on the control of active and reactive power (P-Q) flow in a single phase inverter.

This project was sponsored by the Energy Systems Technology Evaluation Program, US Office of Naval Research.

Furthermore, a novel control strategy is proposed, spanning both stationary and synchronous reference frame, identifying an easy method to implement the entire controller into a field programmable gate array (FPGA). A mixed-frame controller was used in [6] for a single phase inverter operating in islanding mode, however it has not previously been used for grid-connected inverters as we propose here. The advantage is faster execution in a digital controller.

In Section II the active and reactive power flow controller is presented together with the four OGMs. The simulations comparing the controller's performance with different OGMs are presented in Section III. The experimental measurements and validation of the model are presented Section IV. Finally the conclusions are provided in Section V.

II. P-Q Power Control and Orthogonal Generation Methods

This paper focuses on the current-mode controller used when the microgrid is connected to the main grid. In this section the control system represented by the "P-Q Power Control System" box in Fig. 1 is described.

The proposed P-Q controller of the AC source power flow is depicted in the block diagram of Fig. 3 where each step of the control algorithm is represented from left to right, and will be described in detail in this section. One of the novelties of this control scheme is that part of the control is implemented in the Direct-Quadrature (DQ) synchronous frame to ensure the steady state error is zero, while part is implemented in the αβ stationary frame. This mixed-frame control strategy reduces the computational burden on the control hardware.

Controllers implemented in the DQ synchronous reference frame are typically used for three-phase inverters; however, they are also used for single phase inverters by generating fictitious voltages and currents orthogonal to the single phase voltages and currents. As a consequence, in a single phase system, where only one phase exists, a second orthogonal phase has to be created. In this paper, four different methods are used to generate the orthogonal axis components, distinctively affecting the performance of the control strategy. These OGMs are: a) the Quarter Cycle Delay method, b) the Differentiation method, c) the Second Order Generalized Integrator (SOGI) method, and d) the All Pass Filter (APF) method [6].

In Fig. 3 the OGM blocks are used for both voltage and currents; therefore, in the following sections the symbol *X* is used to represent either *V* for voltage or *I* for current. For each of the four different OGMs, Table I presents the time domain and frequency domain equations. In the last column of Table I the transfer function *H(s)* between the α and β components is derived and determined to be equal to –j, therefore proving the orthogonality of the α and β components. In other words, $H(j\omega_o) = -j = 1\angle -90^o$, so when the α-axis component is in the positive horizontal axis (positive x axis), the β-axis is in the negative perpendicular axis (i.e., negative y axis).

A. Quarter Cycle Delay Method

In this method, the α-axis is delayed by one quarter cycle in order to generate the β orthogonal axis. The equations for this method are included in the first row of Table I and their implementation in Simulink is shown in Fig. 2.

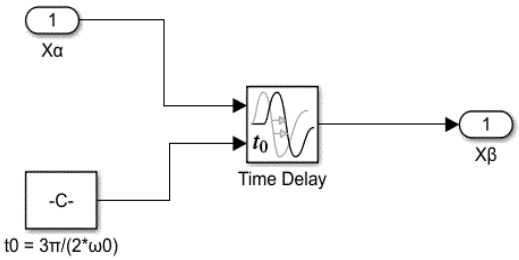

Fig. 2. Simulink block diagram for the Quarter Cycle Delay OGM.

B. Differentiation Method

In this method, the α-axis is differentiated to generate the β orthogonal axis. The equations for this OGM are included in the second row of Table I and their Simulink implementation is shown in Fig. 4.

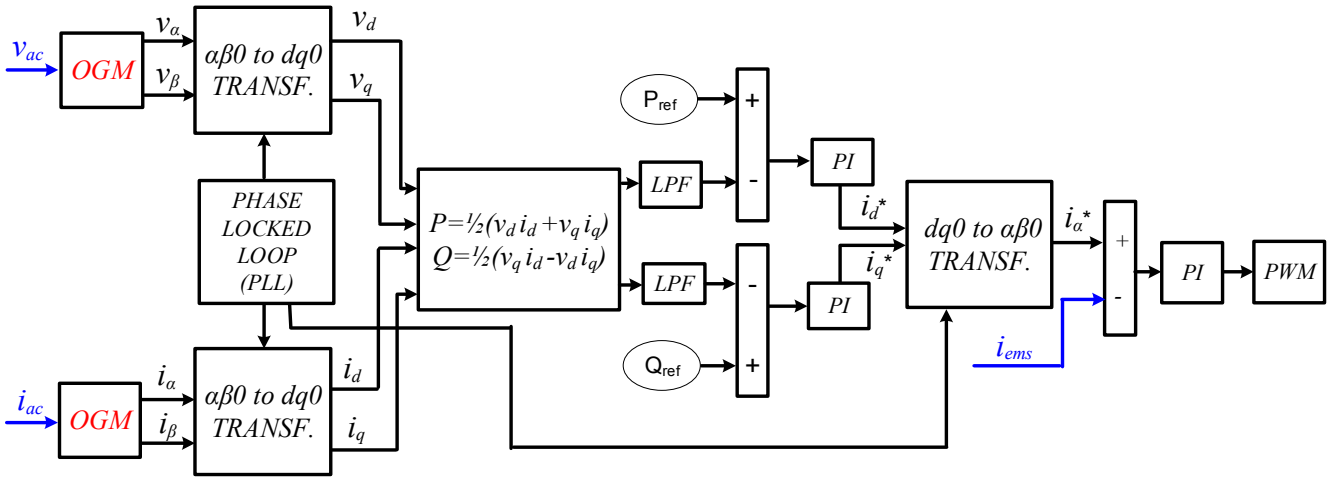

Fig. 3. Block diagram of the novel P-Q source power flow controller.

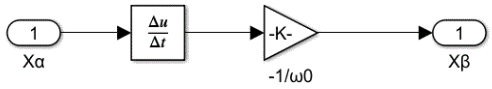

Fig. 4. Simulink implementation of the Differentiation OGM.

C. Second Order Generalized Integrator (SOGI)

By implementing this method, the α-axis component is a filtered input signal of the voltage and current of the main grid, and the generated β-axis component is shifted by 90 degrees with respect to the original components in order to have orthogonality [9]. The equations for this OGM are included in the third row of Table I and their Simulink implementation is shown in Fig. 5.

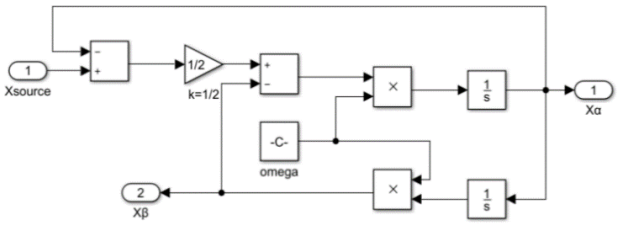

Fig. 5. Simulink block diagram for the SOGI OGM.

TABLE I. ORTHOGONAL GENERATION METHODS (OGM)

OGM	Time Domain	S-domain	Phase Relationship Between α and β axis
QUAR. CYCLE DELAY	$X_\alpha(t)=X_m\sin(\omega_o t)$	$X_\alpha(s)=X_m\frac{\omega_o}{s^2+\omega_o^2}$	$H(s)=\frac{X_\beta(s)}{X_\alpha(s)}=e^{-j\frac{3\pi}{2\omega_o}s}$
	$X_\beta(t)=X_m\sin(\omega_o(t+\frac{3\pi}{2\omega_o}))$	$X_\beta(s)=X_m e^{j\frac{3\pi}{2\omega_o}s}\frac{\omega_o}{s^2+\omega_o^2}$	$H(j\omega_o)=-j$
DIFF.	$X_\alpha(t)=X_m\sin(\omega_o t)$	$X_\alpha(s)=X_m\frac{\omega_o}{s^2+\omega_o^2}$	$H(s)=\frac{X_\beta(s)}{X_\alpha(s)}=-\frac{s}{\omega_o}$
	$X_\beta(t)=-X_m\cos(\omega_o t)$	$X_\beta(s)=-X_m\frac{s}{s^2+\omega_o^2}$	$H(j\omega_o)=-j$
SOGI	$H_1(s)=\frac{X_\alpha(s)}{X_{ac\_source}(s)}=\frac{k\omega_o s}{s^2+k\omega_o s+\omega_o^2}$		$H(s)=\frac{H_2(s)}{H_1(s)}=\frac{X_\beta(s)}{X_\alpha(s)}=\frac{k\omega_o^2}{k\omega_o s}=\frac{\omega_o}{s}$
	$H_2(s)=\frac{X_\beta(s)}{X_{ac\_source}(s)}=\frac{k\omega_o^2}{s^2+k\omega_o s+\omega_o^2}$		$H(j\omega_o)=-j$
APF	$H_1(s)=\frac{X_\alpha(s)}{X_{ac\_source}(s)}=\frac{k_e s-\omega_o k_f}{s^2+k_e s+\omega_o^2-\omega_o k_f}\overset{k_f=-k_e}{=}\frac{k_e(s+\omega_o)}{s^2+k_e s+\omega_o^2+\omega_o k_e}$		$H(s)=\frac{H_2(s)}{H_1(s)}=\frac{X_\beta(s)}{X_\alpha(s)}=\frac{k_e(-s+\omega_o)}{k_e(s+\omega_o)}$
	$H_2(s)=\frac{X_\beta(s)}{X_{ac\_source}(s)}=\frac{k_f s+\omega_o k_e}{s^2+k_e s+\omega_o^2-\omega_o k_f}\overset{k_f=k_e}{=}\frac{k_e(-s+\omega_o)}{s^2+k_e s+\omega_o^2+\omega_o k_e}$		$H(j\omega_o)=\frac{-j\omega_o+\omega_o}{j\omega_o+\omega_o}=\frac{-j+1}{j+1}=-j$

D. All Pass Filter (APF)

In this procedure, a Kalman-based filter is designed [10] and, by selecting the appropriate gains (k_e and k_f), an all pass filter is created. In order to create the two orthogonal axes, the value of k_e has to be equal to $-k_f$. In this paper, the values of gains that used for the simulations are $k_e = 1$ and $k_f = -1$.

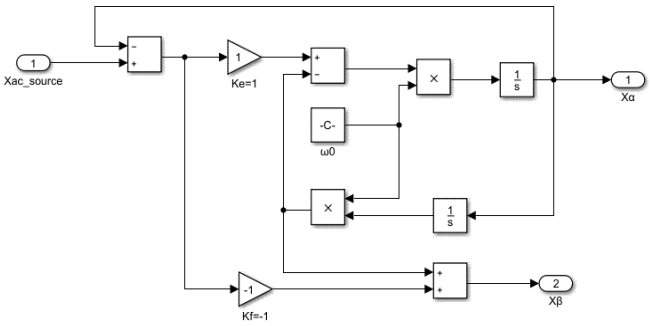

Fig. 6. Simulink block diagram for the APF method.

After the two orthogonal components are created using one of the four methods presented above, the DQ, or Park, transformation is used to create the two DQ components for the voltage (v_d, v_q) and for the current (i_d, i_q):

$$\begin{bmatrix} d \\ q \end{bmatrix} = \begin{bmatrix} \cos(\theta^*) & \sin(\theta^*) \\ -\sin(\theta^*) & \cos(\theta^*) \end{bmatrix} \begin{bmatrix} \alpha \\ \beta \end{bmatrix}. \quad (1)$$

The DQ synchronous reference frame is often used in the analysis of either a single phase or a three-phase system, because the fundamental frequency becomes DC [7] in this reference frame. As a consequence, the analysis of an AC system is simplified by transforming currents and voltages to DC components. This is because "for DC converters it is quite simple to design linear current controllers with no steady state error, but if the AC controllers are designed the same way as DC controllers, a significant steady state error in both amplitude and phase may occur" [8]. Fig. 7 shows a schematic view of the relationship between the α-β and d-q axes, where θ^* is the angle between the two axes.

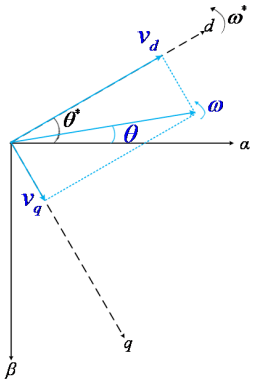

Fig. 7. Axes α-β and d-q [11].

In order to convert the AC voltage of the single phase grid to the desired DC component, the angle between the α-β and d-q axes has to lock to θ^* with a phase-locked loop (PLL). In that way, the d-axis will follow the voltage of the main grid and simultaneously the q-axis voltage will be zero. According to Goldman, a PLL "synchronizes the output phase and frequency of a controllable oscillator to match the output phase and frequency of a reference oscillator. Ideally, the steady-state condition will show a zero difference in phase and frequency between the controlled oscillator output and the reference output" [12]. Fig. 8 shows the αβ0 to dq0 transformation, implementing (1), and the Simulink block diagram of the PLL used to lock the angle θ^* [13]. The q-axis reference voltage is set to zero ($v_q^* = 0$).

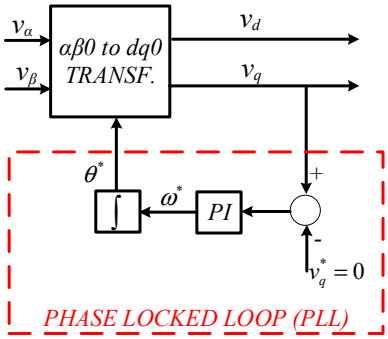

Fig. 8. Synchronous reference frame PLL.

After creating the DQ axis and calculating the two DC components for the voltage (v_d, v_q,) and the two DC components for the current (i_d, i_q), we can calculate the active and reactive power:

$$P = \frac{1}{2}(v_d i_d + v_q i_q), \quad (2)$$

$$Q = \frac{1}{2}(v_q i_d - v_d i_q). \quad (3)$$

The P and Q values computed with (2) and (3) are then filtered by a Low Pass Filter (LPF) and compared to the references, which are the desired values of P and Q.

After the LPF, a Proportional-Integral (PI) controller produces the reference DQ currents i_d^* and i_q^*, which are transformed to the stationary frame into i_α^* and i_β^*. This transformation can be implemented using two different methods. The first method is shown in Fig. 3, where a dq0 to αβ0 transformation is implemented using the angle θ* from the PLL. This is the method used in this paper, however it is worth mentioning that a second method yields the α-β reference frame currents from the following matrix equation [4], [9],[14]:

$$\begin{bmatrix} i_\alpha^* \\ i_\beta^* \end{bmatrix} = \frac{1}{v_\alpha^2 + v_\beta^2} \begin{bmatrix} v_\alpha & v_\beta \\ v_\beta & -v_\alpha \end{bmatrix} \times \begin{bmatrix} P^* \\ Q^* \end{bmatrix} \quad (4)$$

The two methods yield equivalent results in simulations [13] and, since the first method is easier to implement into an FPGA because there are no divisions, it is used in the laboratory prototype.

The final part of the controller, implemented with another PI, is executed in the stationary frame, producing the command voltage signal for the PWM generator. In this PI controller, the input is the error between the reference ($i_\alpha^* = i_{ems}^*$) and the measured EMS current (i_{ems}). This portion of the controller is one of the novel contributions of this paper because in all previous paper addressing grid-connected inverters, this last step of the control algorithm was implemented in the DQ frame as well.

III. Comparing OGMs in Simulations

A physics-based model of the system in Fig. 1 was implemented in Matlab/Simulink and used to simulate different scenarios with the objective of observing how the performance of the P-Q controller varies when different OGMs are used. The circuit in Fig. 9 shows the values of the passive components that were used for the simulations. These values were selected to match the laboratory prototype values, so that the physics-based model can be validated by experimental measurements.

Two models were used to simulate the AC grid voltage: a) an ideal sinusoidal voltage source, and b) a voltage source with harmonics as observed in the laboratory. The first scenario was simulated in order to compare the different OGMs under ideal conditions. For the second scenario the experimental measurements of the AC grid voltage were used to create simulations that could predict the behavior of the controller as implemented on a laboratory prototype. The laboratory voltage spectrum is presented in Fig. 10.

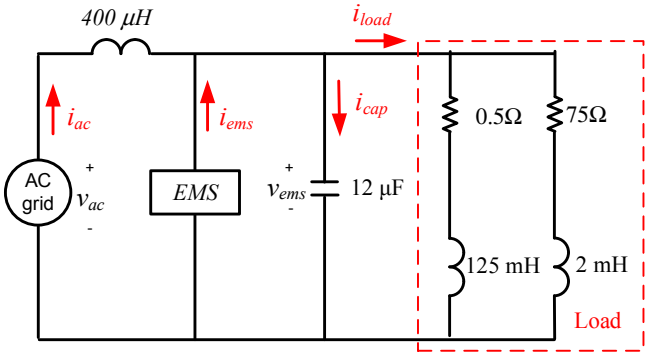

Fig. 9. Simplified electric circuit for EMS testing.

The plots in Fig. 11 show the simulated P and Q obtained with an ideal voltage source and with a non-ideal voltage source. In all cases the average P and Q track their commanded signals, 500W and 0 VARs respectively. The simulation results obtained with all four OGMs are displayed together in Fig. 11 (a) and (c), where the large ripple present when the differentiation method is used covers the other waveforms. Fig. 11 (b) and (d) show the simulation results for the three OGMs, without the differentiation method.

In the ideal source scenario, Fig. 11 (a) and (b) demonstrate that, although the controller works well with all four OGMs, the differentiation OGM presents increased noise with respect to the other cases. In fact, Fig. 11 (b) depicts the three other OGMs, without the differentiation method, indicating that they produce similar results.

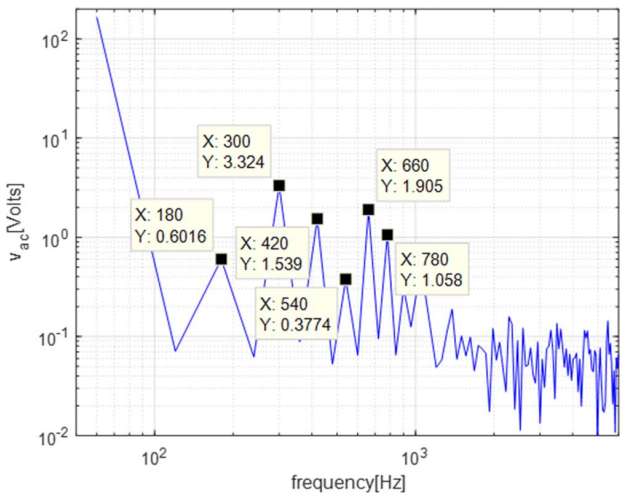

Fig. 10. Experimental measurement of the AC grid voltage spectrum used to create a non-ideal AC voltage source for the simulations.

In the non-ideal source scenario, when a voltage source with harmonics as in Fig. 10 is used, the P-Q controller tracks the commanded values of 500W and 0 VARS with all four OGMs, however the ripple is significant, especially for the differentiation method. It is perceptible in Fig. 11 (d) that the performance of the SOGI method is not affected from the presence of harmonic in the AC grid. This is not the case when the differentiation method is used; a noticeable, significant ripple is present when compared to the simulated results obtained with an ideal AC grid voltage source. The Quarter Cycle Delay and the APF methods result in a small ripple, ten times smaller than the ripple obtained with the differentiation OGM.

The AC source current and voltage are shown to be in phase in Fig. 12, which presents the simulated waveforms obtained with the SOGI OGM. Fig. 12 also presents the EMS current, which is the H-bridge current, produced as a result of the novel P-Q power control presented in this paper. The results for the two scenarios, ideal and non-ideal AC voltage source, are shown Fig. 12 (a) and Fig. 12 (b) respectively. These results show that, while P and Q are tracked accurately, the AC voltage distortion is reflected in the source current.

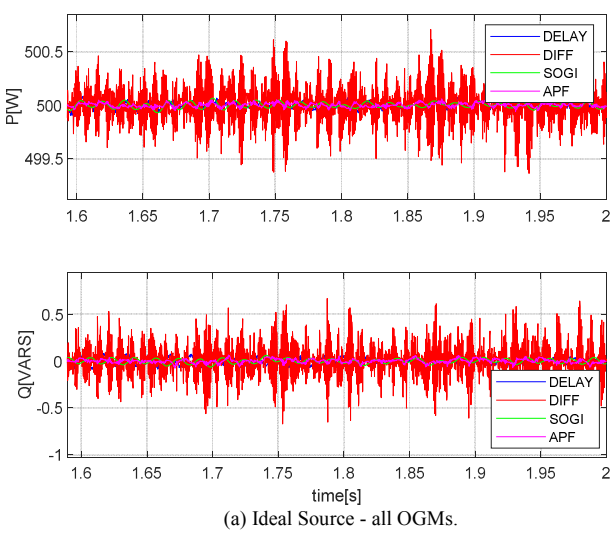

(a) Ideal Source - all OGMs.

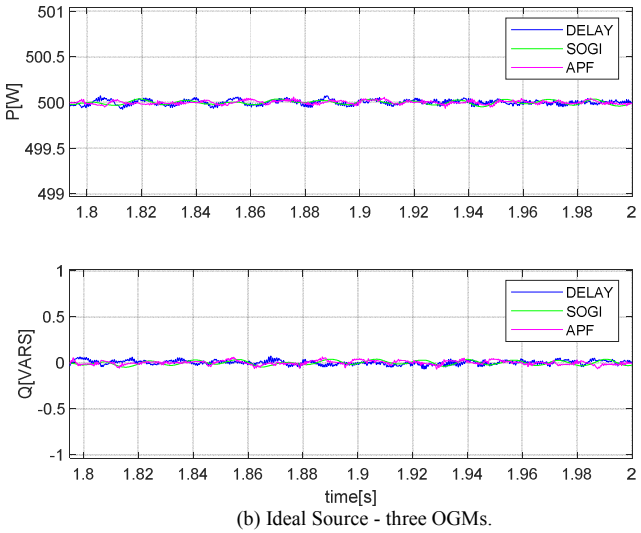

(b) Ideal Source - three OGMs.

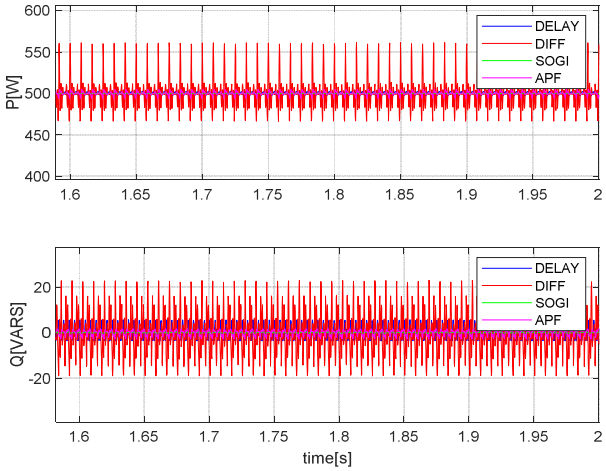

(c) Non-ideal AC Source - all OGMs.

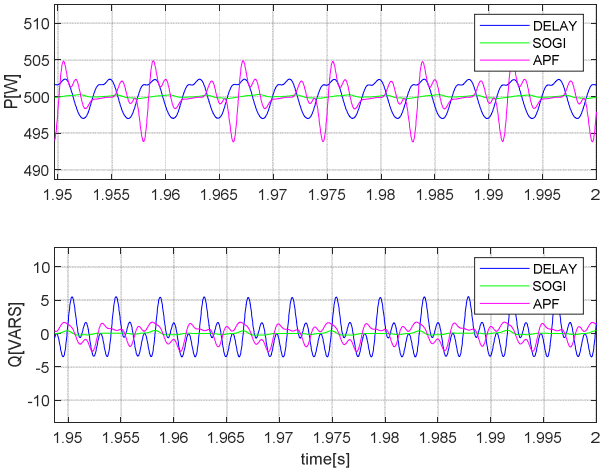

(d) Non-ideal AC Source - three OGMs.

Fig. 11. Steady state simulation plots when P is commanded to 500W and Q to 0 VARS: ideal AC voltage source (a) (b), non-ideal AC voltage source (c) (d).

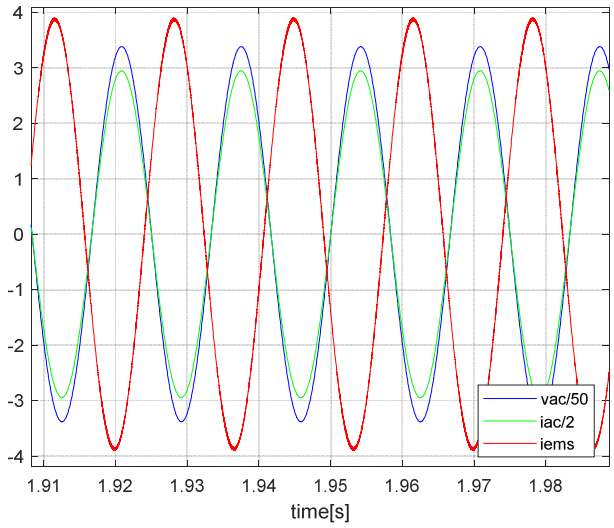

(a) With ideal AC voltage source.

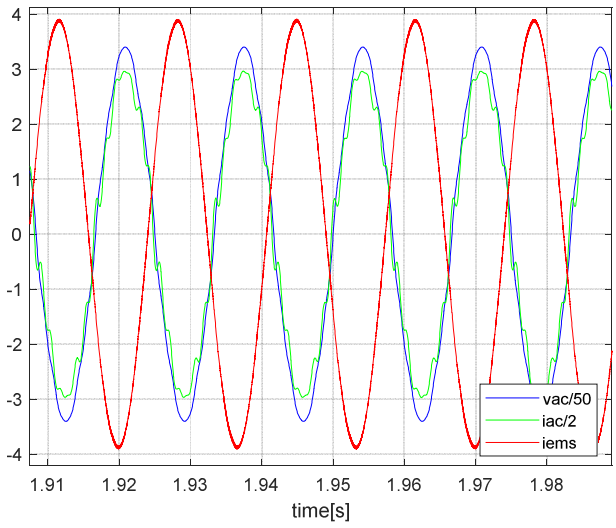

(b) With non-ideal AC voltage source.

Fig. 12. Simulated source voltage, source current and EMS current with SOGI method: (a) ideal source scenario (b) non-ideal source scenario.

IV. Experimental Validation

A laboratory prototype of the EMS was built and is shown in Fig. 13 [1][3]. It includes the following three Printed Circuit Boards (PCBs):

1) The bottom PCB includes the power electronics, passive components, a DC power supply, voltage and current sensors and cooling fans.

2) The FPGA control board is connected to a Personal Computer (PC) through a Join Test Action Group (JTAG) cable [1]. The FPGA is part of a Xilinx development board [15], and is programmed using MATLAB/Simulink and the Xilinx System Generator software [16]. The purpose of this software is to convert the Simulink model into Very High Speed Integrated Circuit Hardware Description Language (VHDL) code. The novel P-Q controller, with the SOGI OGM was programmed into the FPGA board to validate the simulation results.

3) The interface board consists of a number of analog-to-digital converters and many other connections in order to pass signals between the FPGA and the bottom PCB.

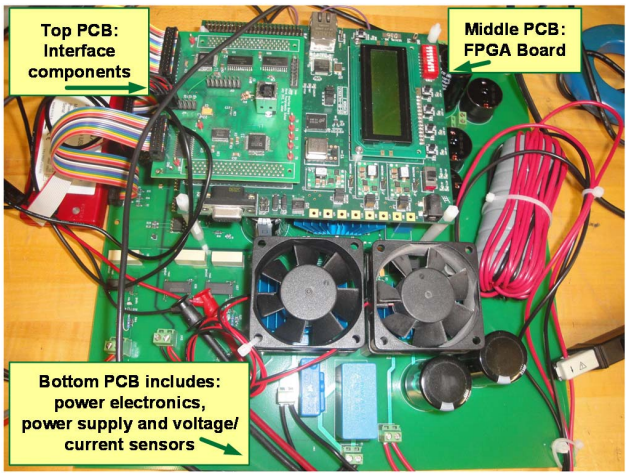

Fig. 13. EMS hardware as implemented in the laboratory.

The laboratory prototype was built as the simulated circuit represented in Fig. 9, with the EMS hardware shown in Fig. 1 and the grid-connected controller shown in Fig. 2 and described in section II. The SOGI OGM with k = ½ was implemented because it demonstrated the best performance in simulations [13]. The experimental plots were acquired using the Xilinx integrated logic analyzer to export the data from the FPGA. Steady state and dynamic response measurements are reported in the following sections.

A. Steady State Measurements

Fig. 14 and Fig. 15 present the steady state experimental measurements when the commanded active power is P = 150 W and the commanded reactive power is Q = 0 VARs. In Fig. 14 we see that the commanded active power and the commanded reactive power are tracked well by the controller, as predicted by the simulations in the previous section. Unity power factor (Q=0 VARs) is confirmed by the waveforms in Fig. 15 where the source current is in phase with the AC source voltage.

B. Step Response

The plots in Fig. 16 present the experimental measurements together with the simulated plots for two commanded steps of the active power, with the reactive power set to Q=0 VARs to achieve unity power factor at the source.

The step from P=150W to P=500W is shown in Fig. 16 (a) with experimental plots and is compared to the simulated plots in Fig. 16 (c). The step from P=500W to P=150W is shown in Fig. 16 (b) with experimental plots and is compared to the simulated plots shown in Fig. 16 (d). In both cases the results demonstrate that the controller tracks the commanded active power quickly and effectively. It is also interesting to notice the disturbance on the reactive power Q, which is kept

constant at 0 VARs. This disturbance is predicted by the simulations, although a small discrepancy can be seen in the step down response. The similarity between experimental and simulated plots validates the physics-based model implemented in Simulink and described in section II.

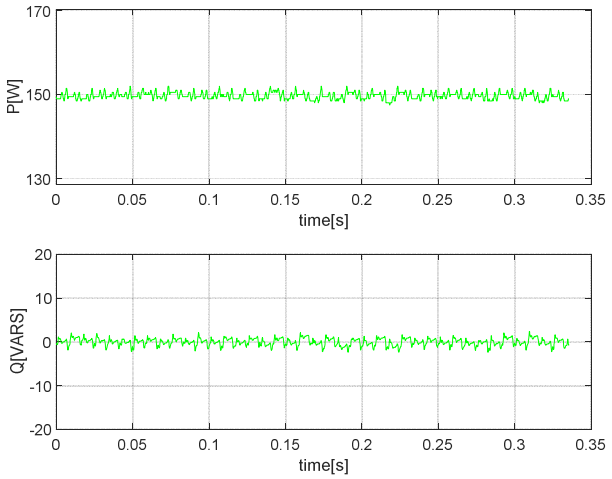

Fig. 14. Experimental validation of the commanded active power P = 150 W and the commanded reactive power Q = 0 VARS.

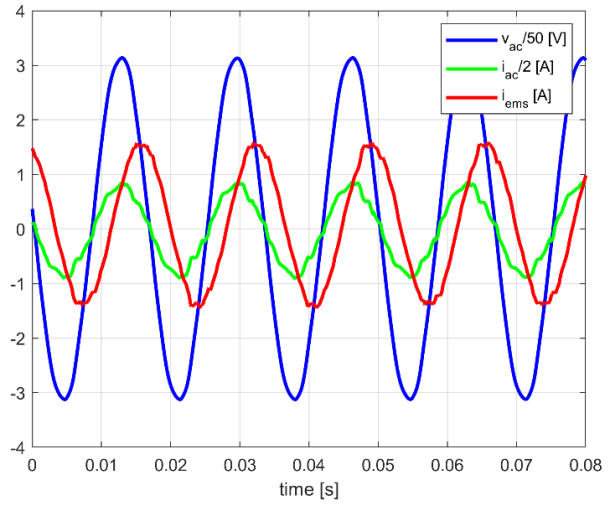

Fig. 15. Experimental measurements of source voltage, source current and EMS current.

V. Conclusions

In this paper we demonstrate the performance of a novel mixed-frame controller for active and reactive power flow control in a single phase grid-connected microgrid. A mixed-frame controller is partially implemented in the DQ frame and part in the stationary frame. In addition we review four different methods for generating the fictitious orthogonal components and we implement them into a physics-based model to evaluate their effect on the controller's performance.

Simulation results demonstrate that when an ideal AC voltage source is used, all OGMs are equivalent. However when a non-ideal voltage source is used, it has an effect on the controller response. The differentiation method is negatively affected and characteristically is the only OGM in which the active power and reactive power cannot be controlled. The Quarter Cycle Delay and the APF OGMs present a slight distortion, in different degrees. The SOGI method yields the best performance and is used for the laboratory implementation.

Experimental measurements on a laboratory prototype, in which the controller was entirely implemented into an FPGA, are presented to demonstrate the functionality of the controller and to validate the simulated results. The physics-based model and simulations were used to support the controller's design, including the SOGI constant k and the parameters of the PI controllers.

References

[1] G. Oriti, A. L. Julian, and N. J. Peck, "Power-electronics-based energy management system with storage," *IEEE Trans. Power Electron.*, vol. 31, no. 1, pp. 452–460, Jan. 2016.

[2] N. Anglani, G. Oriti, and M. Colombini, "Optimized energy management system to reduce fuel consumption in remote military microgrids," *IEEE Trans. Industry Appl.*, vol. 53, no. 6, pp. 5777–5785, Nov.–Dec. 2017.

[3] G. Oriti and A. L. Julian, "Reactive power control with an energy management system in single phase AC microgrids," in *IEEE Energy Convers. Congr. Expo (ECCE)*, 2015, pp.753–759.

[4] R. I. Bojoi, L. R. Limongi, D. Roiu, A. Tenconi, "Enhanced Power Quality Control Strategy for Single-Phase Inverters in Distributed Generation Systems", *IEEE Trans. on Power Electron*., vol. 26, No. 3, pp 798-806, Mar 2011.

[5] J. Rocabert, A. Luna, Frede Blaabjerg, P. Rodrıguez, "Control of power converters in AC microgrids", *IEEE Trans. Power Electron.*, vol. 27, no. 11, pp. 4734–4749, Nov. 2012.

[6] D. Dong, T. Thacker, R. Burgos, F. Wang, D. Boroyevich, "On Zero Steady-State Error Voltage Control of Single-Phase PWM Inverters With Different Load Types", *IEEE Trans. on Power Electron.*, vol. 26, No. 11, pp 3285-3297,Nov.2011.

[7] A. Roshan, R. Burgos, A. C. Baisden, F. Wang, D. Boroyevich "A D-Q Frame Controller for a Full-Bridge Single Phase Inverter Used in Small Distributed Power Generation Systems", in *IEEE 2007 Applied Power Electronics Conference*, 2007, pp.641-647.

[8] U. A. Miranda, M. Aredes, and L. G. B. Rolim, "A DQ synchronous reference frame current control for single-phase converters," *36th Power Electr. Specialists Conf.*, 2005, pp. 1377–1381.

[9] T. Orlowska-Kowalska, F. Blaabjerg, and J. Rodriguez, *Advanced and Intelligent Control in Power Electronics and Drives.* Switzerland: Springer International Publishing, 2014.

[10] K. De Brabandere, T. Loix, K. Engelen, B. Bolsens, J. Van den Keybus, J. Driesen and R. Belmans, "Design and operation of a phase-locked loop with Kalman estimator-based filter for single-phase applications," *32nd Annu. Conf. IEEE Indust. Electr.*, 2006, pp. 525–530.

[11] M. Bobrowska-Rafal, K. Rafal, M. Jasinski, and M. Kazmierkowski, "Grid synchronization and symmetrical components extraction with PLL algorithm for grid connected power electronic converters—A review," *Bull. Polish Acad. Sci.: Tech. Sci.,* 2011, pp. 485–497.

[12] S. Goldman, *Phase-Locked Loop Engineering Handbook for Integrated Circuits*. Boston, MA, USA: Artech House, 2007.

[13] D. Kanavaros, "Implementantion of Active and Reactive Power Flow Control in a Single Phase Microgrid", thesis in partial fulfillment of the Electrical Engineering Degree and MSEE, Naval Postgraduate School, June 2019.

[14] H. Akagi, E. H. Watanabe, and M. Aredes, *Instantaneous Power Theory and Applications to Power Conditioning*. Hoboken, NJ, USA: John Wiley and Sons, 2007.

[15] Xilinx, "Virtex-4 Family Overview," Aug. 30, 2010. [Online]. Available:https://www.xilinx.com/support/documentation/data_sheets/ds112.pdf

[16] Xilinx, "System Generator for DSP—Getting Started Guide," Dec. 02, 2009. [Online]. Available: https://www.xilinx.com/support/documentation/sw_manuals/xilinx11/sysgen_g

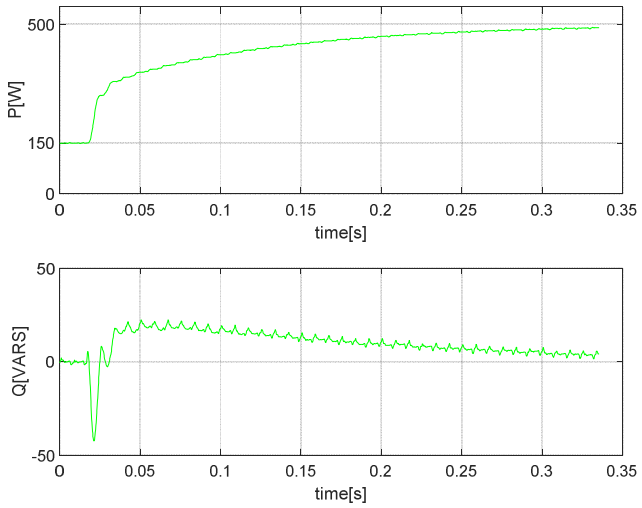

(a) Experimental - step P from 150 W to 500W.

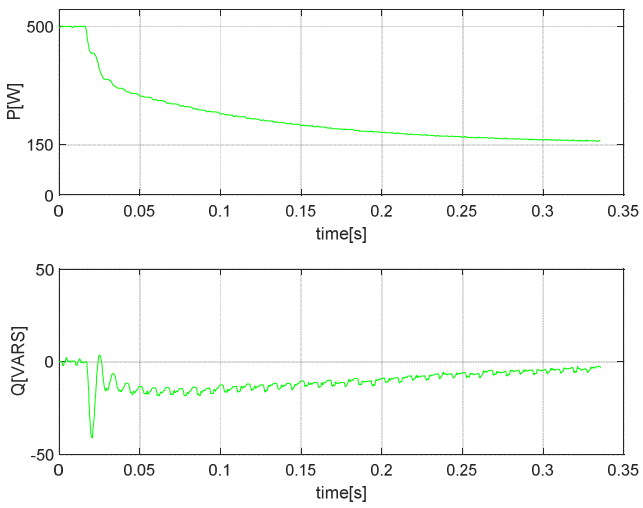

(b) Experimental - step P from 500 W to 150W.

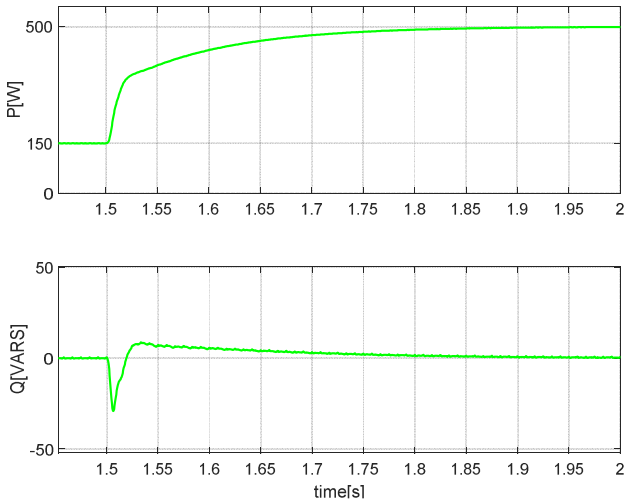

(c) Simulations - step P from 150 W to 500W.

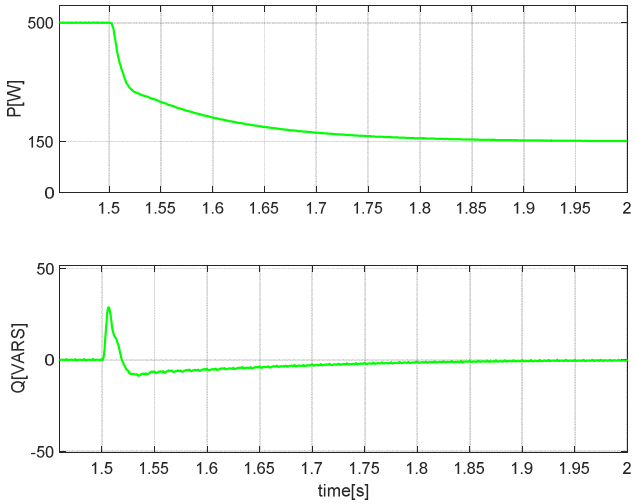

(d) Simulations - step P from 500 W to 150W.

Fig. 16. Experimental validation of the step responses to a change of P , with Q= 0 VARS and comparisong with the simulated results: (a) (c) commanded active power P from 150 W to 500W , (b) (d) commanded active power P from 500 W to 150W.